The Role of Pacific Asian Marginal Seas in modulating the North Pacific Oscillation

Yu-heng Tseng[1], Ruiqiang Ding[2], Sen Zhao[3], Chun Hoe Chow[4]

[1] *Climate and Global Dynamics Laboratory, NCAR, Boulder, Colorado, USA*

[2] *State Key Laboratory of Numerical Modeling for Atmospheric Sciences and Geophysical Fluid Dynamics (LASG), Institute of Atmospheric Physics, Chinese Academy of Sciences, Beijing &*
Plateau Atmosphere and Environment Key Laboratory of Sichuan Province, Chengdu University of Information Technology, Chengdu, China

[3] *Key Laboratory of Meteorological Disaster of Ministry of Education, and College of Atmospheric Science, Nanjing University of Information Science and Technology, Nanjing, China &*
School of Ocean and Earth Science and Technology, University of Hawai'i at Mānoa, Honolulu, USA

[4] *Department of Oceanography, National Sun Yat-sen University, Kaohsiung, Taiwan*

(submitted to ***J. Geophys. Res.-Atmosphere***)

Corresponding author: Dr. Yu-heng Tseng, Climate and Global Dynamics Laboratory, National Center for Atmospheric Research, Boulder, CO80305, USA. Email: ytseng@ucar.edu.

Abstract

We investigate the impact of the Pacific Asian Marginal Sea (PAMS) on the second dominant ocean-atmosphere coupled mode variability in the North Pacific through the modification of North Pacific Oscillation (NPO) variability. The second dominant coupled mode reflects the oceanic footprint of Victoria Mode (VM) forced by the meridional variability of NPO. Our observations show that the November meridional wind in the PAMS strongly connects to the southern lobe variability of the matured NPO in January, leading to the following basin scale oceanic VM pattern. No connection was found for the northern lobe of the NPO. Further wave ray tracing analyses confirmed the above atmospheric teleconnection resulting from the Rossby wave propagation in the middle to upper troposphere. The wave trajectories' origin from the PAMS shows a clear eastward propagating pathway to affect the southern lobe of the NPO from the southern lobe of Western Pacific pattern at 500 hPa on the time scale of one month. No ray trajectories from the lower troposphere can propagate eastward to influence the central-eastern subtropical Pacific. Further analysis suggests that the initialization of the East Asian Winter Monsoon may play an important role in controlling low-level meridional wind variability in the PAMS, but does not explain its completed link with the southern lobe of the NPO.

Keywords: North Pacific Oscillation, East Asian Winter Monsoon, Victoria Mode, Pacific Asian Marginal Seas

1. Introduction

The ocean-atmosphere (O-A) coupled system and its variation in the Pacific show a large impact on global weather and climate. For example, El Niño−Southern Oscillation (ENSO) is a particular mode of Pacific climate variability with strong coupling between the atmosphere and ocean in the tropical Pacific. Several previous studies have found that the teleconnection between the tropics and mid-latitudes may drive ENSO variations through the "Seasonal Footprinting Mechanism" (SFM) proposed by Vimont et al. (2003). The SFM asserts that the second leading pattern of winter atmospheric circulation, the North Pacific Oscillation (NPO), and its variability over the North Pacific can significantly impact spring sea surface temperature (SST) anomalies in the central North Pacific by modifying the wind-stress fields and changing the net surface heat flux over the North Pacific (Vimont et al., 2009; Alexander et al., 2010; Furtado et al., 2012; Ding et al., 2015a; Ding et al., 2015b). Hereafter, the seasons referred to are those occurring in the Northern Hemisphere. The NPO is defined as the second leading mode of winter sea level pressure (SLP) anomalies over the North Pacific (Walker & Bliss, 1932; Rogers, 1981; Vimont et al., 2003; Linkin and Nigam 2008). It consists of a meridional dipole in SLP anomalies, centered near Hawaii and over Alaska. The NPO significantly influences downstream weather and climate conditions over North America during wintertime (e.g., Rogers 1981; Linkin and Nigam 2008). However, its cause and the associated dynamical process modulating its variability are not completely understood.

Most previous studies have stated the variability of NPO is the stochastic atmospheric process (e.g., Rogers, 1981; Furtado et al., 2012). Some studies have recently suggested the nonstationary variability of NPO and its possible connection with the East Asian climate. Wang et al. (2007) found that, before 1975, the NPO was mainly influenced by the ENSO teleconnection with anomalous stationary wave propagation from the subtropical-central Pacific to the northern Pacific. However, after 1975, the NPO was associated with a winter circumglobal wave train pattern over the extratropical region in the Northern Hemisphere and was closely linked to the East Asian climate. Pak et al. (2014) further found another nonstationary relationship between the NPO and the East Asian Winter Monsoon (EAWM) with a sudden change after 1988. This can be associated with the pronounced decadal weakening of the Siberian high system over the Eurasian continent and the eastward migration of the NPO dipole. A strong correlation was found during the 1973-87 strong EAWM epoch, but vanished during the 1988-2002 weak winter monsoon epoch. These studies suggested the complicated dynamics associated with the origin of NPO and how the NPO can be modulated.

Similarly, the impact of the NPO on the ENSO is hardly straightforward. Some studies noted that the existence of negative (positive) NPO in winter(0) does not always result in El Niño (La Niña) the following winter [winter(1)] (Pegion and Alexander, 2013; Ding et al., 2015a). Hereafter, we denote the year in which the El Niño (La Niña) developing year 0 and the preceding and following years as year(-1) and year(1), respectively. The impact of the NPO on the development of ENSO conditions through the SFM may depend on the state of the tropical Pacific (e.g., Anderson, 2007; Alexander et al., 2010; Ding et al., 2015a). Ding et al. (2015a) further confirmed that there is no direct connection between the NPO and ENSO variations. However, the basin-scale oceanic Victoria Mode (VM, Bond et al., 2003), defined as the second leading mode of north Pacific SST anomalies, may act as a more effective pathway for NPO-like atmospheric variability to drive ENSO variability via the SFM. The well-known Pacific Meridional Mode (PMM, Chiang & Vimont, 2004; Chang et al., 2007), which directly links to the SFM, is merely a partial response of the basin-scale VM (see the detailed discussion in Ding et al., 2015a).

Indeed, better connection of the basin-scale VM to the ENSO variation than PMM (or NPO) mode suggests the active role of the Western North Pacific (WNP). Figure 1 shows the correlation map of Niño4 index in January(1) and Pacific SST anomalies at different lags (only correlation coefficients significant at the $p < 0.05$ level are shown) from Extended Reconstructed SST version 4 (ERSST.v4) observations (1948–2015). The Niño4 index is chosen here because it closely relates to the central Pacific warming (CPW) commonly excited by the PMM (e.g., Yu and Kim 2011; Kim et al. 2012; Vimont et al., 2014). Similar patterns and correlations can be found using Niño3 or Niño3.4 indices. The evolution pattern shows the different developing stages of VM before the mature phase of ENSO. We note that a good correlation between the SST anomalies and Niño4 index can be identified in the WNP and eastern Indian Ocean more than nine months prior (left panel). The correlation is higher than 0.6 (significant at the $p < 0.05$ level) at the 12-month lead time in the WNP. This high correlation region (signals already emerged at the 15-month lead time) is located at the southern edge of the WNP index defined in Wang et al. (2012)

and may directly trigger the winter(0) SST dipole in the WNP, which is related to the development of ENSO in the following winter(1). Similar patterns can also be found in the Hadley Centre SST data set (not shown).

The above high correlation in the WNP is supported by several other regional studies that have also noted SST anomalies in the marginal seas of the WNP are colder than normal monthly climatology in the developing years [year(0)] of El Niño. Hong et al. (2001) found that summer(0) SST anomalies in the East (Japan) Sea tend to be colder than during year(-1) prior to the developing year [year(0)]. SST anomalies during El Niño developing years are also opposite to those during La Niña developing years. Similar cold SST anomalies in spring(0) have been further confirmed based on three independent long-term observational stations off the east coast of South Korea (Jo et al., 2014). These signals of cold SST anomalies in the WNP are consistent with the correlation map in Figure 1.

In particular, Wang et al. (2012) used the winter(0) SST anomaly dipole to enhance the ENSO forecast. A strong correlation between ENSO and the preceding SST anomalies dipole in the Pacific Asian Marginal Seas (PAMS) of the WNP was found based on a robust statistical analysis (similar to Figure 1). They thought that the spatial pattern in the WNP shares similar characteristics with the MM (Chiang & Vimont, 2004; Chang et al., 2007; Zhang et al., 2009), except that the meridional SST anomalies gradient and low-level zonal wind anomalies occur in the western tropical Pacific. These studies strongly suggested that large-scale SST anomalies over the subtropical/extratropical WNP are significantly related to El Niño 12 months later through the modulation of the winter NPO and can be used as a useful predictor for El Niño development. However, it remains unclear as to how these regional WNP findings are linked to the NPO and the forced basin-scale VM.

In this paper, we focus on the pathway modulating the NPO-like atmospheric variability (specifically the southern Lobe) from the PAMS. We isolate the dominant role of the WNP (originating primarily from the PAMS) and its influence on the winter NPO variability. The driving mechanism and pathway modulating the NPO will be addressed by means of observation and the Rossby wave ray tracing analyses. Section 2 introduces the observational data and the Rossby wave ray tracing method theory. Section 3 investigates the modulation of the NPO variability resulting from the WNP in the observation. Section 4 validates the associated pathway using the Rossby wave ray tracing. Section 5 discusses how this PAMS origin explains the

ENSO precursor signals in the literature. Finally, conclusions and suggestions for further work are provided in Section 6.

2. Data, analysis method and theory

2.1 Observational data

Three observational datasets for the period 1948–2015 are used here. The monthly SLP, surface wind components, surface latent heat flux, geopotential height, and wind vectors are taken from the National Centers for Environmental Prediction – National Center for Atmospheric Research (NCEP–NCAR) reanalysis project (Kalnay et al., 1996; Kistler et al., 2001) on a 2.5°×2.5° horizontal grid resolution and 12 vertical pressure levels ranging from 1000 to 100 hPa. The climatology of 1986–2015 is removed. For the surface latent heat flux, we also verify the dynamical processes discussed in this paper using objectively analyzed air-sea fluxes, OAFLUX (Yu et al., 2008), during 1983–2009. Some minor differences can be found in the amplitude; however, there is no significant difference in terms of the patterns comparing with the NCEP–NCAR reanalysis product. Therefore, for the sake of consistency, we present all observational results based on NCEP–NCAR reanalysis throughout the paper. The ERSST.v4 data are taken from the National Climatic Data Center on a 2°×2° horizontal grid (Smith et al., 2008). All relevant SST indices are calculated from the ERSST.v4 data based on the standard definition. The representation of the NPO is defined according to the second dominant SLP anomalies mode in the combined empirical orthogonal function (CEOF) analysis (Tseng et al., 2016a). The linear trend is removed for all datasets.

2.2 Rossby wave ray tracing theory

Rossby wave ray tracing theory can provide comprehensive insights into the wave evolution and has been shown to effectively characterize the subsequent evolution of the Rossby wave train excited by the tropical heating source (Hoskins and Karoly 1981; Shaman and Tziperman 2005; Zhao et al., 2015). Following Li et al. (2015) and Zhao et al. (2015), the dispersion equation for propagation of Rossby wave on a horizontally non-uniform flow with the inclusion of the meridional component may be written as,

$$\omega=\overline{u}_M k+\overline{v}_M l+\frac{l\,\partial\overline{q}/\partial x-k\,\partial\overline{q}/\partial y}{K^2}, \tag{1}$$

where ω is the frequency, $\left(\overline{u}_M,\overline{v}_M\right)=\left(\overline{u},\overline{v}\right)/\cos\varphi$ is the Mercator projection of the basic-state zonal and meridional winds, $\overline{q}=2\Omega\sin\varphi+\nabla^2\overline{\psi}$ is the basic-state absolute vorticity, φ is latitude, Ω is the rotation rate of the earth, and $\overline{\psi}$ is the basic-state streamfunction; $K=\sqrt{k^2+l^2}$ is the total wavenumber, k and l are the zonal and meridional wavenumbers, respectively. The wave ray is defined as a trajectory that is locally tangential to the group velocity. Using the Eq. (1), the group velocity of the Rossby wave packet takes the form

$$u_g=\overline{u}_M+\left[\left(k^2-l^2\right)\partial\overline{q}/\partial y-2kl\,\partial\overline{q}/\partial x\right]\Big/K^4 \quad \text{and} \tag{2a}$$

$$v_g=\overline{v}_M+\left[2kl\,\partial\overline{q}/\partial y+\left(k^2-l^2\right)\partial\overline{q}/\partial x\right]\Big/K^4 . \tag{2b}$$

The evolutions of wavenumbers k and l along a trajectory are determined by kinematic wave theory (Whitham 1960), as follows

$$\frac{d_g k}{dt}=-k\frac{\partial\overline{u}_M}{\partial x}-l\frac{\partial\overline{v}_M}{\partial x}+\frac{k\,\partial^2\overline{q}/\partial y\partial x-l\,\partial^2\overline{q}/\partial x^2}{K^2} \quad \text{and} \tag{3a}$$

$$\frac{d_g l}{dt}=-k\frac{\partial\overline{u}_M}{\partial y}-l\frac{\partial\overline{v}_M}{\partial y}+\frac{k\,\partial^2\overline{q}/\partial y^2-l\,\partial^2\overline{q}/\partial x\partial y}{K^2}, \tag{3b}$$

where $d_g/dt=\partial/\partial t+u_g\,\partial/\partial x+v_g\,\partial/\partial y$ represents the material derivative moving with the group velocity.

For each initial zonal wave number k and an initial position within the region where the wave source has been perturbed, we use Eq. (1) to solve for the initial meridional wavenumber l by assuming $\omega=0$ (stationary waves). Then Eqs. (2) and (3) were integrated to derive the ray trajectory; they were terminated when the spatial scale of Rossby waves was less than 1000 km. The background climatological mean wind flow is based on the November-December-January (NDJ) NCEP-NCAR reanalysis for the period of 1963-2015. Since the Wentzel-Kramers-Brillouin approximation used in the Rossby wave theory also requires a slow-varying background flow (Li et al., 2015), we also smoothed the background flows of $\overline{u}$ and $\overline{v}$ by multiplying a spherical harmonic component with total wavenumber n by $\exp\left\{-\xi\left[n\left(n+1\right)\right]^2\right\}$, where the coefficient ξ has been set such that the harmonic component of n = 16 was reduced by 37%. This reduced the potential impacts of the small-scale structures in the basic state. Further examination indicates that the results are not sensitive to the smoothing method applied. Further details can be found in Li et al. (2015) and Zhao et al. (2015).

3. Link between the surface meridional winds in the PAMS and the NPO

Figure 1 suggests the ENSO variability is connected with the precursory spring Pacific VM and its atmospheric forcing of NPO (Ding et al., 2015a). These surface expressions can be well explained using the second dominant CEOF (CEOF2) of SLP and SST anomalies in the Pacific (Figure 2). The meridional dipole structure of SLP anomalies in the North Pacific is the typical signature of the NPO pattern (Figure 2a). This NPO pattern is very similar to that reported earlier (Linkin & Nigam, 2008; Furtado et al., 2012) and is a robust winter atmospheric feature. There is another weak pressure low in the subtropical WNP, which has drawn only minor attention (Anderson, 2007), but may be important to modulate the NPO variability (discussed in section 5). The CEOF2 of the SST anomalies resembles the VM described above (Bond et al., 2003; Di Lorenzo et al., 2008; Ding et al., 2015a)—a region of negative SST anomalies extending from the WNP to the Kuroshio Extension, encircled by warm SST anomalies around the North Pacific coast reaching the central tropical Pacific (Figure 2b). The variability of CEOF2 is directly connected to the most recent warm Blob observed in the Northeastern Pacific evolved from late 2013 to 2016 and the persistence of the 2014/15 North Pacific climate linking to the strong 2015 El Niño (Di Lorenzo and Mantua, 2016; Tseng et al., 2016a). However, these recent studies only address the evolution of the VM in the El Niño events and the multi-year enhancement (Figure 1c-1f). They did not address the preceding SST anomalies observed in the PAMS [winter(0)] one year in advance of the occurrence of El Niño (Figure 1b), which may link to the development of the NPO and the following evolution of VM.

Based on the observational evidences (e.g., Wang et al. [2012] and Figure 1), we propose the local atmospheric heating related to the SST dipole in the PAMS can affect the NPO developing phase through the atmospheric teleconnection during the early winter (i.e., November-December-January, NDJ). The teleconnection can be initiated from the change of alongshore wind in the East Asian (discussed in section 5), particularly the meridional wind component. Figure 3 shows the correlation map of the November surface meridional wind anomaly in the PAMS (120~140°E, 5~25°N), hereafter referred to as "V_{PAMS}", with several lags of SLP anomalies (0 to 3 months). Prior to the correlation analysis, the Niño3.4 index was linearly removed from the wind fields using the regression. The removal of the Niño3.4 index from the data ensures that the surface meridional winds are independent of any ENSO variability that occurs simultaneously in the tropical Pacific. This region is chosen from the largest SST anomalies correlation map 12 months prior to the mature phase of ENSO shown in Figure 1b. The results are not sensitive if a slightly larger region is selected (e.g., 100~140°E, 5~30°N) as long as the high correlation area in Figure 1b is included. The simultaneous large correlation can be found along the coast of China from South China Sea (SCS) to Yellow Sea (maximum negative correlation R=-0.73), indicating the strong geostrophic wind balance. Another comparable largest correlation can be found when the November V_{PAMS} leads the SLP anomalies by 2 month (R=0.56) in the region just above the southern branch of the VM (defined as SLP_S, 180°~140°W, 5~25°N, see the grey box in the Figure 1c). This is the region where the southern lobe of the NPO starts to initiate the VM or MM through the SFM (Ding et al., 2015a). Furtado et al. (2012) suggested a large distinction in the dynamics between the northern and southern lobes of the NPO while the southern lobe of the NPO likely linked to the CPW. This viewpoint is supported by the significant correlation in Figure 3c, while the correlation is not significant for the northern lobe of the NPO. Our results suggest a more direct impact of the PAMS surface wind variability in modulating the NPO within two months than the low-frequency influence proposed by Furtado et al. (2012).

The two-month lag near the southern lobe of the NPO is not a coincidence. Figure 4a verifies the observed lead-lag correlation between the V_{PAMS} and the SLP anomalies in the southern branch of the VM region (the grey box in the Figure 1c), i.e., influencing the southern lobe of the NPO. Our results suggest that any potential heating source in the PAMS can affect the central-subtropical Pacific two months later. Another significant, but weaker, correlation can be found in March when SLP anomalies in the southern branch of the VM region has no lag with the V_{PAMS}. This simultaneous correlation is actually associated with the spring footprint of VM resulting from the NPO forcing and supports the main difference between the VM and MM (discussed in Ding et al., 2015a). Figure 4b shows a similar lead-lag correlation between the V_{PAMS} and the PC2 associated with CEOF2 (NPO/VM) pattern described above. Note that a minus sign is applied to the PC2 to ensure the consistency of the correlation sign. As expected, a clearer correlation can be found, indicating the PC2 actually leads the V_{PAMS} in spring, causing the basin-scale VM pattern. The triggering of NPO on the ENSO development is not only through the MM but also affects the surface wind in the PAMS. Since this spring-to-summer evolution has been detailed previously, our current study emphasizes the winter development of the NPO.

The correlation analysis suggests the enhanced November V_{PAMS} in the PAMS leads to the growth of winter NPO, reaching its maximum in January (particularly the southern lobe). The NPO then forces the surface SST footprint of VM through the SFM, which matures in the following March or April (Ding et al., 2015a). Figure 5a shows the time series of the November $-V_{PAMS}$, January $-SLP_S$ and the March PC2, respectively. Negative signs of V_{PAMS} and SLP_S are included here to be consistent with the phase of CEOF2 and its associated PC2 shown in Figure 2. The variation between the November $-V_{PAMS}$ and January $-SLP_S$ matches reasonably well, especially after 2000. The corresponding years which have magnitudes greater than one standard deviation are also listed in Table 1.

Figure 6 further shows the correlation map between the November V_{PAMS} with the geopotential height anomalies (top three panels: 200 hPa, 500 hPa, and 1000 hPa, respectively) for November and two consecutive lag months (December and January). The simultaneous large positive/negative correlation in November is clear at 1000 hPa along the coast of China, covering Southeast Asia (consistent with Figure 3), while the positive correlation offshore in the WNP can further extend up to 200 hPa. This suggests a northward wind in the PAMS can be associated with a zonal dipole of cyclonic and anticyclonic eddies near the surface, resulting from a local heating source (the same correlation map with latent heat flux is also shown at the bottom). The upward extension to the mid and upper troposphere can be supported by the similar correlation map with the vertical velocity, Ω, in November (upward vertical motion corresponds to the negative Ω) in Figure 7. The upward motion is also consistent with the region of negative OLR anomalies above the PAMS in Figure 8a, corresponding to the anomalously strong convection and rainfall. The phenomenon is reversed for the equatorward meridional velocity in the PAMS (i.e., $-V_{PAMS}$). These results suggest a barotropic structure is formed in November associated with the surface meridional wind in the PAMS, which is connected to the January NPO pattern in the eastern North Pacific.

This atmospheric teleconnection may likely result from the Rossby wave train. In

December, the remote atmospheric teleconnection associated with the November V_{PAMS} starts to emerge and evolve in the eastern North Pacific (middle panel in Figure 6). The largest correlation occurs in the correlation map of January over the southern branch of the VM in the lower troposphere. This is also associated with a positive correlation in the Ω at 500 hPa and 200 hPa (right panel in Figure 7), suggesting a strong response on the SLP anomalies. These results show a propagating atmospheric teleconnection in the mid to upper troposphere which affects the southern lobe of NPO.

4. Rossby wave train mechanism

In order to further explore the described pathway to modulate the winter NPO from the PAMS, we used a theoretical wave ray tracing approach to analyze the potential atmospheric teleconnection resulting from the PAMS during the NDJ. These theoretical analyses examine if the subsequent evolution of the Rossby wave train excited by the heating source from the PAMS can further influence the eastern North Pacific (thus the strength of NPO). Figure 9 shows the wave ray trajectories initiated by the heating sources (crosses) over the PAMS regions under the climatological 500 hPa basic flows and integrated for 20 days. The initial position arrays (110°E~140°E and 5°N~30°N, slightly larger than the domain specified in Figure 1b) over the PAMS region were selected to represent the impact of the source locations on the wave propagation. The results shown here are for both positive and negative initial meridional wavenumber l to reflect initially northward and southward propagation of stationary waves, respectively.

Interestingly, the sources over the northern PAMS region (north of 20°N) can indeed excite two branches of waves that propagate eastward to the North Pacific sector: the northern branch is poleward and reflected equatorward at mid-latitudes (about 60°N for $k=2$). The other southern branch is equatorward and reflected poleward at the latitudes where the zonal winds equal zero ($U = 0$; about 20°N). A major part of the northern branch finally arrives in the central-eastern North Pacific over the southern branch of the VM before moving eastward to the American continent. Trajectories based on the initial zonal wavenumbers $k=4$ and $k=6$ exhibit qualitatively similar paths, except waves with a larger zonal wavenumber can propagate higher latitudes before equatorward reflection. These two branches of waves confine the wave activity to the North Pacific sector and confirm the sources over the PAMS region can potentially modulate the NPO variability after 20 days, specifically the southern lobe over the southern branch of the VM. This central-eastern North Pacific region is also consistent with the largest correlation between November V_{PAMS} and the January (also December but weaker) geopotential height at 500 hPa shown in Figure 6. Based on the NDJ climatological winds, our integration of wave ray equations indicates the energy transfer from the PAMS source locations can reach the south lobe of NPO in 20 days, which approximately resemble to the 1-2 month lag shown above.

In contrast, the sources over the southern part of the PAMS region (south of 20°N) cannot excite waves that can spread eastward. All trajectories are moving westward into tropical western Pacific. This suggests that the north-south locations in the PAMS are critical to determine their impacts. Only the sources within the southern lobe of Western Pacific (WP) teleconnection pattern (i.e., north of about 20°N) (Wallace and Gutzler, 1981; Chow et al., 2016) can influence the Southern lobe of NPO, consistent with the strong connection between the WP and NPO patterns (Linkin and Nigam, 2008).

Similar wave ray trajectories can also be found at 250 hPa (Figure 10) but the number of trajectories reaching the central-eastern North Pacific is reduced. More trajectories recirculate anti-cyclonically at 250 hPa than 500 hPa for $k=2$ (i.e., belonging to the sources over the southern part of the PAMS). This is mainly because the vertical structure of the WP tilts northward with increased altitudes (similar to the November correlation map shown in the left panel of Figure 6). Also, the wave trajectories affecting the southern lobe of the NPO are reflected at lower latitudes at 250 hPa than 500 hPa, as the jet stream is stronger in 250 hPa leading to the lower turning latitudes.

The trajectories are entirely different in the low troposphere. Nearly all rays propagate westward and cannot propagate to the central-eastern North Pacific under the 850 hPa circulation condition (Figure 11). This results from the enhanced southwestward EAWM during the NDJ month. In general, our wave ray tracing analysis, consistent with the NDJ observation shown in section 3, provides evidences that the source in PAMS can significantly contribute to the variability of NPO pattern through the Rossby wave propagation. We find the impact is strongest between

600-400 hPa during the NDJ background flow configurations and is directly related to the southern lobe of winter WP pattern. We note that only the stationary waves are discussed here because of the climatological winds, where the disturbances propagate as the group velocity with zero phase velocity stationary.

5. Discussion

A new pathway was proposed and verified between the PAMS and the NPO during the winter, one that offers a new perspective on the assumed stochastic dynamics of NPO. Past studies on the NPO have focused mainly on the impacts of its teleconnection patterns on the weather and climate of North America (Linkin & Nigam, 2008) and how the NPO initiates ENSO through the SFM (Ding et al., 2015a; Ding et al., 2015b). Most studies looking at the NPO-induced SFM focus on the consequent changes of surface and subsurface heat content in the central-eastern tropical Pacific (e.g., Anderson, 2004; Anderson & Maloney, 2006; Anderson, 2007). Only a few studies have emphasized the origin of NPO variability. The modulation of NPO due to the V_{PAMS} we describe here mostly affects the NPO's southern lobe (near Hawaii over the southern branch of the VM) prior to the NPO-induced SFM. This is confirmed by the observation and the theoretical wave ray tracing analyses. The influence is similar to the finding of low-frequency forcing of CPW in modulating the low-frequency mode of the NPO in Di Lorenzo et al. (2010) and Furtado et al. (2012). However, we point out a more direct impact of the PAMS surface wind variability in modulating the southern lobe of the NPO through the Rossby wave train propagation on the time scale of one month.

Our results confirmed that the variability of January NPO southern lobe can be controlled by the November V_{PAMS} in the PAMS. This regional surface wind change is highly associated with the SST anomalies heating source in the PAMS (R=0.58). Similar lag correlation maps based on the November SST index defined in Wang et al. (2012) are superimposed in Figure 3 as thick dashed contours (blue and red dashes represent R=0.5 and 0.4, respectively). The spatial patterns are quite similar to the maps based on the November V_{PAMS}. However, the impact of SST anomalies on the NPO southern lobe appears weaker than the impact of November V_{PAMS} (lower correlation). Wang et al. (2012) implied that the surface winds in the WNP occur almost at the same time as the NPO from December to February (Figure 4 in Wang et al., 2012). Based on the monthly observational data (instead of three-month mean) in section 3 and wave ray tracking analyses in section 4, we further clarify that the NPO can be intensified through the middle to upper tropospheric Rossby wave propagation from the WNP. The November V_{PAMS} plays an important role in enhancing the growth of the southern lobe of the NPO, thus forcing the following basin-scale SST footprint of spring VM in the North Pacific. This is indeed consistent with the tight connection between the WP and NPO (Linkin and Nigam 2008). Recent analysis suggested the WP and NPO to be essentially the same variability, with the NPO being the sea level pressure reflection of the WP geopotential height pattern (Nigam 2003; Linkin and Nigam 2008; Nigam and Baxter 2015). Here, we further demonstrate the origin of the NPO and WP variability is linked with the heating source in the PAMS.

The V_{PAMS} in the PAMS can be viewed as the trigger-forcing of the tropical–extratropical teleconnection associated with the NPO variability through the Rossby wave propagation. However, many factors can influence its variability. Further analysis of the 11-yr running correlation coefficient between the V_{PAMS} and southern lobe of NPO variability confirmed that the two indices were well correlated after late 1970s with increasing correlation after 2000 (Figure 5b) and poorly correlated during early 1960s and mid-1970s, consistent with the nonstationary connection with the EAWM and the intensified circumglobal wave train activity after 1975 (Wang et al., 2007; Pak et al., 2014). The identified PAMS is a region where the thermal contrast between the East Asian continent and the Pacific is important while the EAWM plays a pivot role in the winter climate.

We found the response of November V_{PAMS} that we define here varies simultaneously with the SCS winds and extends northward to the east edge of the Ryukyu Islands with a correlation larger than 0.85 (Figure 8b). A one-month lag correlation map of December suggests the November V_{PAMS} intensifies the local cyclonic circulation over the maritime continent (Figure 8c), thus leading to the eastern Pacific teleconnection pattern in January (Figure 8d). It also lags behind the East China Sea and the Japan Sea winds along the coast of China (25~50°N) by 1 month (R>0.5). These results suggest that the along-coast wind (mostly meridional wind) associated with the initiation of EAWM in the PAMS during the early winter may modulate the NPO variability. We could not find any available EAWM indices well correlated with the V_{PAMS}. The matured EAWM may have a different inherent dynamics so that the EAWM may not be the only dynamic process to control the V_{PAMS}.

In addition, the formation of V_{PAMS} (or the along-coast wind) may be partially caused by the shape of the East Asian coasts and partially related to the pressure gradient between the Siberian high and the Maritime Continent low (Wang & Chen, 2014). The variability of subtropical high in the WNP may also contribute to V_{PAMS}. It is possibly the variability of V_{PAMS} is the result of the competition between the EAWM and the WNP subtropical high. Unfortunately, we have not yet found a well-defined WNP subtropical high index to confirm this. The circulation variability near the WNP subtropical high may also connect with the triggering pressure low shown in the CEOF2 pattern (Figure 2a) (also found in Anderson, 2004; 2007). The simultaneous November correlation map of V_{PAMS} also shows such a high correlation feature collocated with the pressure low anomaly (Figure 6g). In terms of the link to the following winter(1) El Niño development, it is likely the ocean dynamics, combined with the impact of initiating EAWM, may change the local O-A interaction, thus contributing to the enhanced -V_{PAMS} through the latent heat release (Figure 6j). For example, the preconditioned Warm Water Volume (WWV) in the recharge–oscillator mechanism reflects the associated oceanic responses and the subsurface changes to precondition the Pacific WWV (as do WWB, e.g., Fedorov, 2002) more than one year ahead of the ENSO events (Chen et al., 2015).

The development of ENSO events may require both the trigger from the south lobe of the NPO and the ocean subsurface preconditioning (Tseng et al., 2016b). In general, the local O-A interaction in the PAMS due to the underlying ocean precondition resulting from the Pacific Subtropical Cell circulation may be a key triggering mechanism that affects V_{PAMS}, which then modulates the variability of southern lobe of NPO. But this process requires a more detailed investigation of the subsurface dynamics.

There are some additional mechanisms that could potentially excite the thermodynamic heating/cooling source in the PAMS to affect ENSO variability. For example, Chang et al. (2009) found that significant negative (positive) SST anomalies in the WNP appear in the strong (weak) Subtropical Mode Water (STMW) case. Their statistical analysis indicated that summer(-1) STMW variability can also affect ENSO events 18 months later. They suspected that summer STMW(-1) variability produces subtropical atmospheric variability through long-term persistent SST anomalies over its reemergence area to derive the VM pattern, and eventually modulates the amplitude of ENSO events; however, the role of the STMW still needs to be clarified.

Moreover, our results are consistent with previous evidence linking the Tsushima Warm Current to the NPO reported by Hirose et al. (2009). They showed that changes in the Tsushima Warm Current (a current fed by the Kuroshio, which passes between Korea and Japan) during autumn were correlated with the following winter NPO/WP pattern. The surface wind stress in the PAMS indeed controls the transport of Kuroshio and its branches due to the Sverdrup circulation. The consequent response of atmospheric circulation to the Kuroshio can also be found through a positive feedback process in the WNP (Qiu & Chen, 2010; Shen et al., 2014; Chow et al., 2016). The intensive coupled O-A interaction in the WNP significantly modulates the North Pacific climate variability.

6. Conclusion and future work

The origin of the well-known extratropical NPO forced upon ENSO is investigated and its possible pathway originating from the PAMS have been analyzed in this study using the observation and the wave ray tracing analyses. The NPO commonly forces the basin-scale VM, leading to a matured O-A coupled mode of variability in the subtropical North Pacific (i.e., CEOF2). The proposed pathway well explains all northern hemispheric precursors of El Niño in the literature related to the NPO/VM and the link of PAMS one year in advance (Figure 1). We confirm the origin from the V_{PAMS} modulating the NPO/VM variability. The schematic in Figure 12 summarizes a possible explanation of dynamical processes linking the PAMS origin and the onset of El Niño. The variability of the southern lobe of the NPO is initiated by the change of V_{PAMS} associated with the surface heating, and then the reduced deep convection propagates northeastward through the Rossby wave propagation, thus enhancing the deep convection (also reducing the subsidence) near the southern branch of the VM. This is followed by a typical negative phase of NPO forced VM in the Northern Hemisphere (Ding et al., 2015a; Ding et al., 2015b) forming the combined SLP and SST anomalies pattern of CEOF2 from spring(0) to summer(0). The enhanced westerly wind can further lead to the onset of El Niño by the changing of Walker circulation.

We found the enhanced (reduced) November deep convection associated with V_{PAMS} aligns well with the changes of southern lobe of the November WP and January subsidence in the central-eastern subtropical Pacific. These processes are robust regardless of the length of the analysis years. This directly supports the integrated picture of the WP and NPO characterized in Linkin and Nigam (2008) but we specifically point out their WNP origin. The wave propagation is on a one-month time scale. We found no evidence of the impact of NPO on the WNP until spring when the basin-scale VM emerges (Ding et al., 2015a).

The wave ray tracing analyses confirm the proposed pathway described in the observation. The wave rays origin from the PAMS show clear eastward propagating trajectories reaching the central-eastern subtropical Pacific over the southern branch of the VM (near the southern lobe of the NPO) in the middle to upper troposphere, similar to the typical Rossby wave propagation. These are totally opposite to the wave ray trajectories in the lower troposphere, which flow mostly westward and never reach eastern Pacific. Both the observation and wave raying tracing analyses show no link of the PAMS heating source with the northern lobe of the NPO in the dynamical processes while the abovementioned atmospheric teleconnection affects primarily on the southern lobe of the NPO.

The initiation of EAWM seems to play an important role in controlling a part of the variability of V_{PAMS} but does not explain its completed link with the southern lobe of the NPO. The nonstationary relationship between the EAWM and NPO can also be connected through the variability of V_{PAMS}. Our results suggest a seasonally dependent O-A interaction in the PAMS, possibly linked to the change of subtropical high in the WNP. The November V_{PAMS} acts as a pivotal driver to modulate the NPO/VM (meridional variability) through the atmospheric teleconnection. However, the detailed O-A interaction involved is still not clear, specifically the heating source of SST anomalies. Further investigations into the relevant O-A interaction in the PAMS are planned using the linear baroclinic models and CESM-forcing sensitivity studies.

REFERENCES

Alexander, M. A., D. J. Vimont , P. Chang, and J. D. Scott, 2010: The impact of extratropical atmospheric variability on ENSO: Testing the seasonal footprinting mechanism using coupled model experiments. *J. Clim.*, **23**, 2885–2901.

Anderson, B. T., and E. Maloney, 2006: Interannual tropical Pacific sea surface temperatures and their relation to preceding sea level pressures in the NCAR CCSM2. *J. Clim.*,**19**, 998–1012.

Anderson, B. T., 2004: Investigation of a large-scale mode of ocean–atmosphere variability and its relation to tropical Pacific sea surface temperature anomalies. *J. Clim.*, **17**, 4089–4098.

Anderson, B. T., 2007: On the joint role of subtropical atmospheric variability and equatorial subsurface heat content anomalies in initiating the onset of ENSO Events. *J. Clim.*, **20**, 1593–1599.

Bond, N. A. , J. E. Overland, M. Spillane, and P. Stabeno, 2003: Recent shifts in the state of the North Pacific. *Geophys. Res. Lett.*, **30**, 2183, doi:10.1029/2003GL018597.

Chang, P., L. Zhang, R. Saravanan, D. J. Vimont, J. C. H. Chiang, L. Ji, H. Seidel, and M. K. Tippett, 2007: Pacific meridional mode and El Niño-Southern Oscillation. *Geophys. Res. Lett.*, **34**, L16608, doi:10.1029/2007GL030302.

Chang, R., Q. Y. Zhang, and R. F. Li, 2009: North Pacific premonitory sign of the ENSO event. *Geophys. Res. Lett.*, **36**, L03818, doi:10.1029/2008GL036597.

Chen, H. C., C. H. Sui, Y. H. Tseng, and B. H. Huang, 2015: An analysis of climate oscillations in Pacific subtropical cells. *J. Clim.,* **28**, 3786–3805.

Chiang, J. C. H., and D. J. Vimont, 2004: Analogous Pacific and Atlantic meridional modes of tropical atmosphere-ocean variability. *J. Clim.*, **17**, 4143–4158.

Chow, C.H., Y.H. Tseng, H.H. Hsu and C.C. Young, 2016: The interannual variability of the subtropical countercurrent's eddies in the North Pacific associated with the

Western-Pacific teleconnection pattern, *Cont. Shelf Res.*, doi:10.1016/j.csr.2016.08.006.

Di Lorenzo, E., N. Schneider, K. M. Cobb, P. J. S. Franks, K. Chhak, A. J. Miller, J. C. McWilliams, S. J. Bograd, H. Arango, E. Curchitser, T. M. Powell, and P. Rivière, 2008: North Pacific Gyre Oscillation links ocean climate and ecosystem change. *Geophys. Res. Lett.*, **35**, L08607, doi:10.1029/2007GL032838.

Di Lorenzo, E., K. M. Cobb, J. C. Furtado, N. Schneider, B. T. Anderson, A. Bracco, M. A. Alexander, and D. J. Vimont, 2010: Central Pacific El Niño and decadal climate change in the North Pacific. *Nature Geosci.*, **3**, 762–765.

Di Lorenzo, E. and N. J. Mantua, 2016: Multi-year persistence of 2014/15 North Pacific marine heatwave. *Nature Clim. Change*, doi:10.1038/nclimate3082.

Ding, R., J. Li, Y. H. Tseng, C. Sun, and Y. Guo, 2015a: The Victoria mode in the North Pacific linking extratropical SLP variations to ENSO. *J. Geophys. Res.*, doi: 10.1002/2014JD022221.

Ding, R., J. Li, Y. H. Tseng and C. Ruan, 2015b: Influence of the spring Victoria mode in the extratropical North Pacific on the Pacific summer ITCZ. *J. Geophys. Res*, doi: 10.1002/2014JD022364.

Fedorov, A.V., 2002: The response of the coupled tropical ocean-atmosphere to westerly wind bursts. *Q. J. Roy. Meteorol. Soc.*, **128**, 1–23.

Furtado, J. C., E. Di Lorenzo, B. T. Anderson, and N. Schneider, 2012: Linkages between the North Pacific Oscillation and central tropical Pacific SSTs at low frequencies. *Clim. Dyn.*, **39**, 2833–2846.

Hirose, N., K. Nishimura, and M. Yamamoto, 2009: Observational evidence of a warm ocean current preceding a winter teleconnection pattern in the northwestern Pacific. *Geophys. Res. Lett.*, **36**, L09705.

Hong, C. H., K. D. Cho, and H. P. Kim, 2001: The relationship between ENSO events and sea surface temperature in the East (Japan) Sea. *Prog. Oceanogr.*, **49**, 21–40.

Hoskins, B. J., and D. J. Karoly, 1981: The Steady linear response of a spherical atmosphere to thermal and orographic forcing. *J. Atmos. Sci.*, **38**, 1179–1196.

Jo, Y. H., L. C. Breaker, Y. H. Tseng, and S. W. Yeh, 2014: A temporal multiscale analysis of the water off the east coast of South Korea over the past four decades. *Terr. Atmos. Ocean Sci.* **25**, 415–434.

Kalnay, E., M. Kanamitsu, R. Kistler, W. Collins, D. Deaven, L. Gandin, M. Iredell, S. Saha, G. White, J. Woollen, Y. Zhu, A. Leetmaa, R. Reynolds, M. Chelliah, W. Ebisuzaki, W. Higgins, J. Janowiak, K. C. Mo, C. Ropelewski, J. Wang, R. Jenne, and D. Joseph, 1996: The NCEP/NCAR 40-Year Reanalysis Project. *Bull. Amer. Meteor. Soc.*, **77**, 437–471.

Kim, S. T., J.-Y. Yu, A. Kumar, and H. Wang, 2012: Examination of the two types of ENSO in the NCEP CFS model and its extratropical associations. *Mon. Wea. Rev.*, **140**, 1908–1923.

Kistler, R., E. Kalnay, W. Collins, S. Saha, G. White, J. Woollen, M. Chelliah, W. Ebisuzaki, M. Kanamitsu, V. Kousky, H. van den Dool, R. Jenne, and M. Fiorino, 2001: The NCEP–NCAR 50-Year Reanalysis: Monthly Means CD–ROM and Documentation. Bull. *Amer. Meteor. Soc.*, **82**, 247–267.

Li, Y., J. Li, F. F. Jin, and S. Zhao, 2015: Interhemispheric propagation of stationary Rossby waves in the horizontally nonuniform background flow. *J. Atmos. Sci.*, **72**, 3233-3256.

Linkin, M. E., and S. Nigam, 2008: The North Pacific Oscillation–West Pacific teleconnection pattern: mature-phase structure and winter impacts. *J. Clim.*, **21**, 1979–1997.

Nigam, S. and S. Baxter, 2015: Teleconnections. Encyclopedia of Atmospheric Sciences, 2nd ed. G. North, Ed., Elsevier Science, 90–109.

Pak G, Y-H. Park, F. Vivier, Y-O Kwon and K-I Chang, 2014: Regime-dependent nonstationary relationship between the East Asian winter monsoon and North Pacific Oscillation. *J. Clim.* **27**, 8185–8204.

Pegion, K., and M. Alexander, 2013: The seasonal footprinting mechanism in CFSv2: Simulation and impact on ENSO prediction. *Clim. Dyn.*, **41**, 1671–1683.

Qiu, B., and S. Chen, 2010: Interannual variability of the north Pacific subtropical countercurrent and its associated mesoscale eddy field. *J. Phys. Oceanogr.*, **40**, 213–225.

Rogers, J. C., 1981: The North Pacific Oscillation. Int. *J. Clim.*, **1**, 39–57.

Shaman, J., and E. Tziperman, 2005: The effect of ENSO on Tibetan Plateau snow depth: A stationary wave teleconnection mechanism and implications for the South Asian monsoons. *J. Clim., **18***, 2067-2079.

Shen, M. L., Y. H. Tseng, S. Jan, C. C. Young, and M. D. Chiou, 2014: Long-term variability of the Kuroshio transport east of Taiwan and the climate it conveys. *Prog. Oceanogr.*, **121**, 60–73.

Smith, T. M., R. W. Reynolds, T. C. Peterson, and J. Lawrimore, 2008: Improvements to NOAA's historical merged land-ocean surface temperature analysis (1880–2006). *J. Clim.*, **21**, 2283–2296.

Tseng, Y.H., R. Ding and X.-M. Huang, 2016a: The warm blob in the northeastern Pacific-the bridge leading to the 2015 El Niño *(submitted to Environmental Research Letters).*

Tseng, Y.H., Z.Z. Hu, R. Ding and H.C. Chen, 2016b: An ENSO prediction approach based on ocean conditions. *Clim. Dyn.* doi: 10.1007/s00382-016-3188-2.

Vimont, D. J., J. M. Wallace, and D. S. Battisti, 2003: The seasonal footprinting mechanism in the Pacific: Implications for ENSO. *J. Clim.*, **16**, 2668–2675.

Vimont, D. J., M. Alexander, and A. Fontaine, 2009: Mid-latitude excitation of tropical variability in the Pacific: The role of thermodynamic coupling and seasonality. *J Climate*, **22**, 518–534.

Vimont, D. J., M. A. Alexander, and M. Newman, 2014: Optimal growth of central and east Pacific ENSO events. *Geophys. Res. Lett.*, **41**, 4027–4034.

Walker, G. T., and E. W. Bliss, 1932: World Weather V. *Memoir. Roy. Meteorol. Soc.*, 4, 53–84.

Wallace, J. M., and D. S. Gutzler, 1981: Teleconnections in the geopotential height field during the northern hemisphere winter. *Mon. Wea. Rev.*, **109**, 784–812.

Wang, L., W. Chen, and R. Huang, 2007: Changes in the variability of North Pacific Oscillation around 1975/1976 and its relationship with East Asian winter climate. *J. Geophys. Res.*, **112**, D11110.

Wang, S. Y., and M. L'Heureux, and H. H. Chia, 2012: ENSO prediction one year in advance using western North Pacific sea surface temperatures. *Geophys. Res. Lett.*, **39**, L05702.

Yu, L., X. Jin, and R. A. Weller, 2008: Multidecade Global Flux Datasets from the Objectively Analyzed Air-sea Fluxes (OAFlux) Project: Latent and sensible heat fluxes, ocean evaporation, and related surface meteorological variables. Woods Hole Oceanographic Institution, OAFlux Project Technical Report. OA-2008-01, 64pp. Woods Hole. Massachusetts.

Yu, J.Y., and S.T. Kim, 2011: Relationships between extratropical sea level pressure variations and the central Pacific and eastern Pacific Types of ENSO. *J. Clim.*, **24**, 708–720.

Zhang, W., J. Li, and F. F. Jin, 2009: Spatial and temporal features of ENSO meridional scales. *Geophys. Res. Lett.*, **36**, L15605, doi:10.1029/2009GL038672.

Zhao, S., J. Li, and Y. Li, 2015: Dynamics of an interhemispheric teleconnection across the critical latitude through a southerly duct during boreal winter. *J. Clim.*, **28**, 7437-7456.

Table 1: corresponding years of November -V_{PAMS} , January -SLP_S and March PC2 which have magnitudes greater than one standard deviation

	>1 standard deviation	<-1 standard deviation
November -V_{PAMS}	1958, 1961, 1968,1975, 1978, 1988, 1989, 1992, 1994, 2004, 2009	1950, 1952, 1953,1954, 1966, 1986, 1987, 1997, 1998, 2006, 2008, 2011
January -SLP_S	1956, 1959, 1968, 1969, 1971, 1972, 1980, 1990, 2005, 2010	1951, 1953, 1955, 1958, 1964, 1984, 1987, 1999, 2001, 2009, 2012, 2016
March PC2	1956, 1957, 1963, 1965, 1968, 1969, 1981, 1985, 1991, 1997, 2005, 2014, 2015	1953, 1983, 1987, 1998, 1999, 2000, 2007, 2008, 2016

Figure captions

Figure 1. The correlation of Pacific SST anomalies (based on 3-month running mean) and January(1) Niño4 index at different lags from 1948–2015. The Niño4 index has lags of (a) 15 months; (b) 12 months; (c) 9 months; (d) 6 months; (e) 3 months; and (f) 0 months (no lag). Only $p<0.05$ is shown. The contour lines correspond to $R=0.6$ (bold black), 0.5 (thin black) and 0.4 (grey). The grey box in (b) shows the specific PAMS region and the grey box in (c) shows the southern branch of the VM.

Figure 2 The CEOF2 of SLP (hPa) and SST (°C) anomalies and the corresponding PC2 in the North and tropical Pacific Ocean. (a) SLP; (b) SST; (c) PC2.

Figure 3. Correlation map of the November surface meridional wind anomaly (V_{PAMS}) in the PAMS with several lags of SLP anomalies (0 to 3 months); (a) November (no lag), (b) December, (c) January and (d) February. See Figure 1 for the description of contour lines. The SST index defined in Wang et al. (2012) is shown as the grey box in (a). Additional thick dashed contours represent similar lag correlations of SLPa with the November SSTa index (Wang et al., 2012) for $R= 0.5$ (blue) and 0.4 (red).

Figure 4. Observed lead–lag correlation between the monthly meridional wind anomalies in PAMS (110~140°E, 5~25°N) and (a) the SLP_S and (b) -PC2, respectively. The SLP_S represents the SLP anomalies in the grey box shown in Figure 1c. See text for the detailed definition of the SLP_S and -PC2. $p<0.05$ is shaded.

Figure 5. (a) Time series of November equatorward meridional wind anomalies ($-V_{PAMS}$) in the PAMS (superimposed by January $-SLP_S$ and March PC2, respectively). All time series are aligned with their corresponding months. Black solid (dashed) lines label the El Niño (La Niña) years in December. (b) 11-yr running correlation coefficient between November V_{PAMS} and January SLP_S. The horizontal line indicates the 95% confidence level.

Figure 6. Correlation maps between November meridional wind anomalies (V_{PAMS}) in PAMS and the geopotential height anomalies (top three panels: 200 hPa, 500 hPa and 1000 hPa, respectively) for November and two lag months (December and January). The same correlation maps with latent heat flux at different lag months are shown at the bottom panel. Only $p<0.05$ is shown.

Figure 7. Same as Figure 6 but for the vertical velocity (Ω) anomalies in November (no lag) and January (two month lag).

Figure 8: Same as Fig. 6 but for the November OLR anomalies and meridional wind anomalies. Regressions of surface winds onto the V_{PAMS} are superimposed. $p<0.05$ is shown as black.

Fig. 9. The stationary Rossby wave ray trajectories (green curves) with initialed zonal wavenumber $k = 2, 4, 6$ (upper, middle, bottom) under the NDJ (right panels) 500 hPa climatological flows (gray vectors) for the period of 1965-2012. Red forks over pink shadings denote wave source arrays over the PAMS region (110°E-140°E, 5°N-30°N).

Fig. 10. Same as Fig.9, but for the 250 hPa climatological flows.

Fig. 11. Same as Fig.9, but for the 850 hPa climatological flows.

Figure 12. Schematic diagram of the dynamical processes linking the PAMS origin and the onset of El Niño. The SLP (contours) and SST (color) anomalies associated with CEOF2 patterns are overlaid.

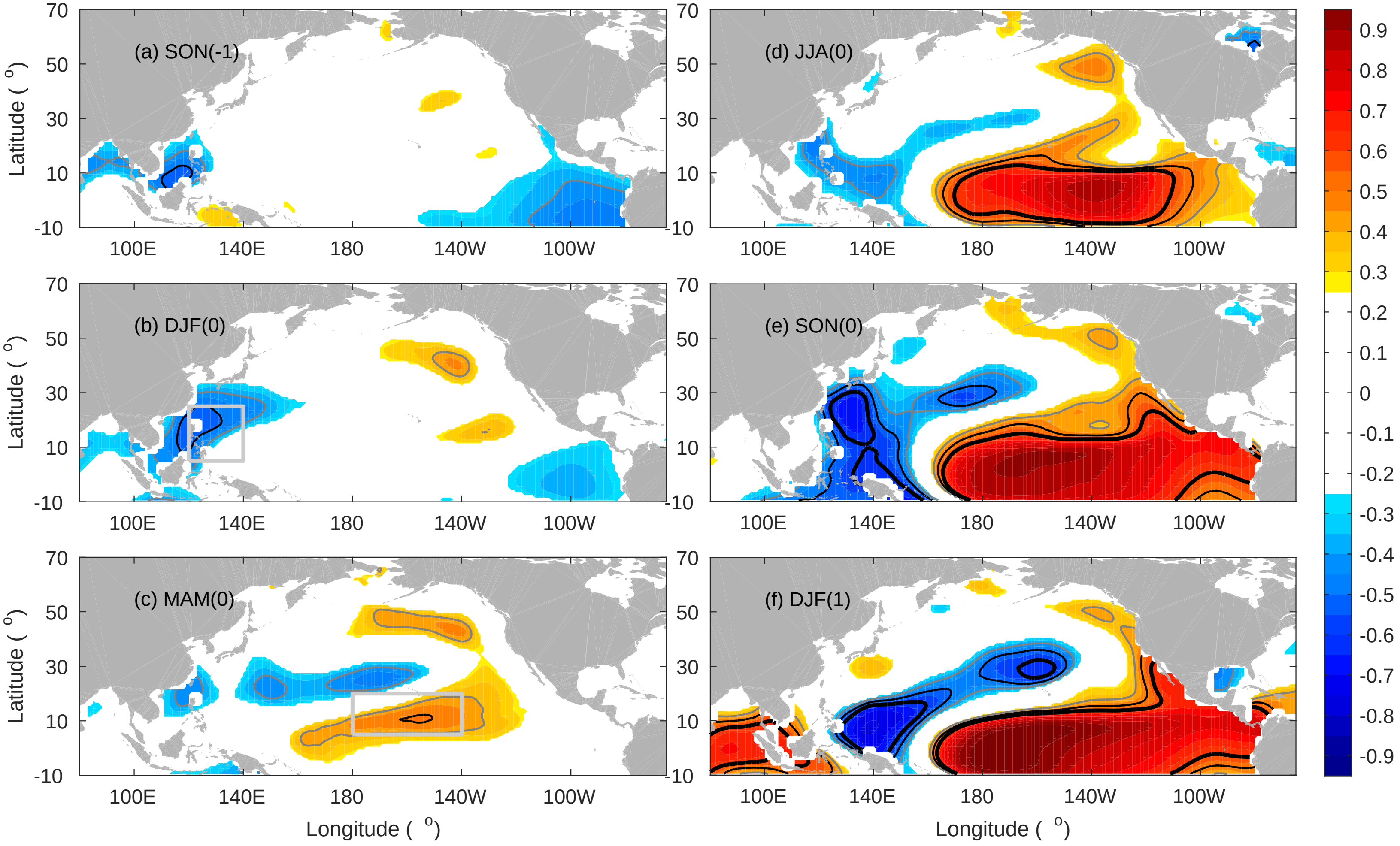

Figure 1. The correlation of Pacific SST anomalies (based on 3-month running mean) and January(1) Niño4 index at different lags from 1948–2015. The Niño4 index has lags of (a) 15 months; (b) 12 months; (c) 9 months; (d) 6 months; (e) 3 months; and (f) 0 months (no lag). Only $p<0.05$ is shown. The contour lines correspond to $R=0.6$ (bold black), 0.5 (thin black) and 0.4 (grey). The grey box in (b) shows the specific PAMS region and the grey box in (c) shows the southern branch of the VM.

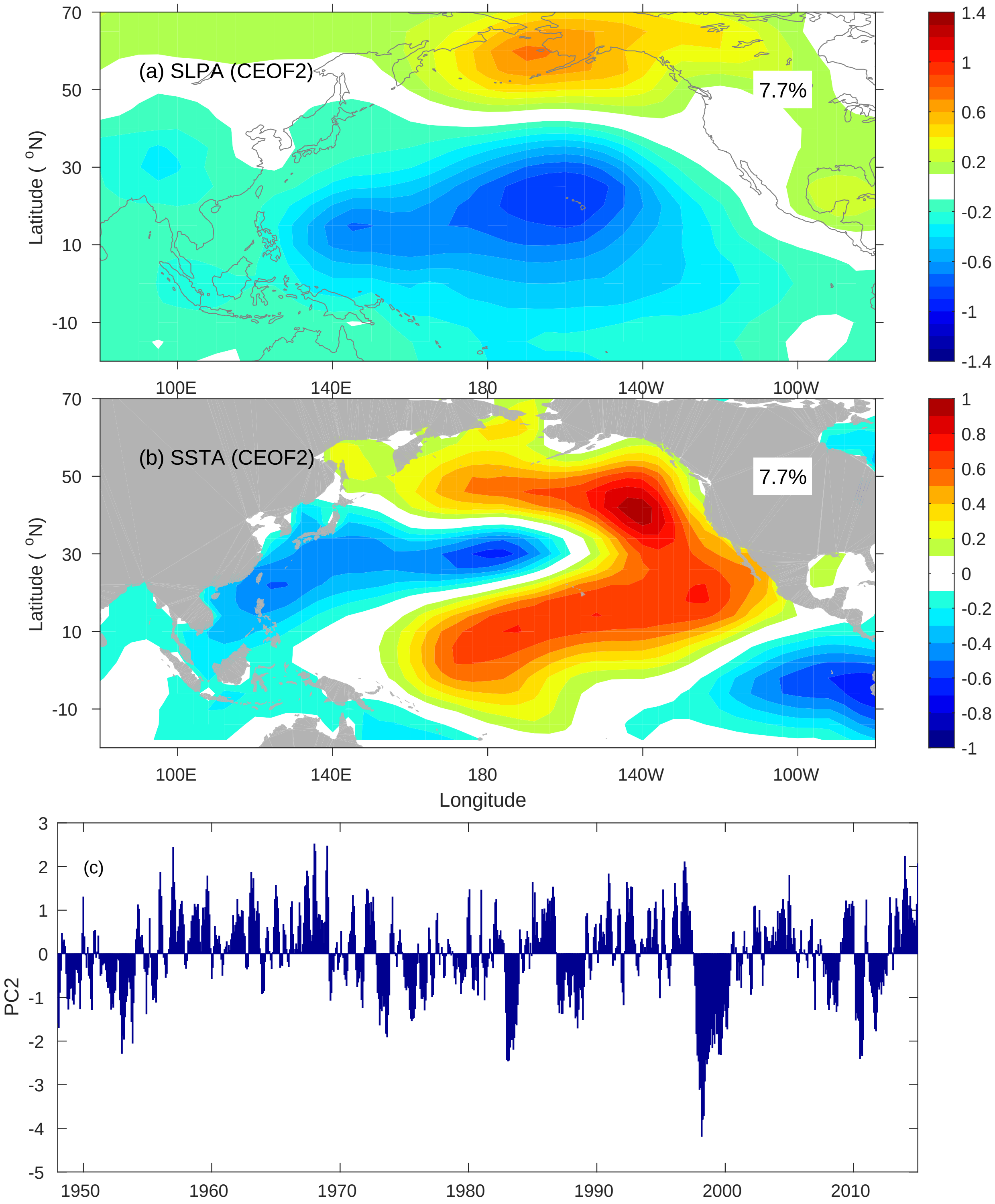
(a) SLPA (CEOF2)
7.7%
70
50
30
10
-10
Latitude (°N)
100E
140E
180
140W
100W
1.4
1
0.6
0.2
-0.2
-0.6
-1
-1.4
(b) SSTA (CEOF2)
7.7%
1
0.8
0.6
0.4
0.2
0
-0.2
-0.4
-0.6
-0.8
-1
Longitude
(c)
PC2
3
2
1
0
-1
-2
-3
-4
-5
1950
1960
1970
1980
1990
2000
2010

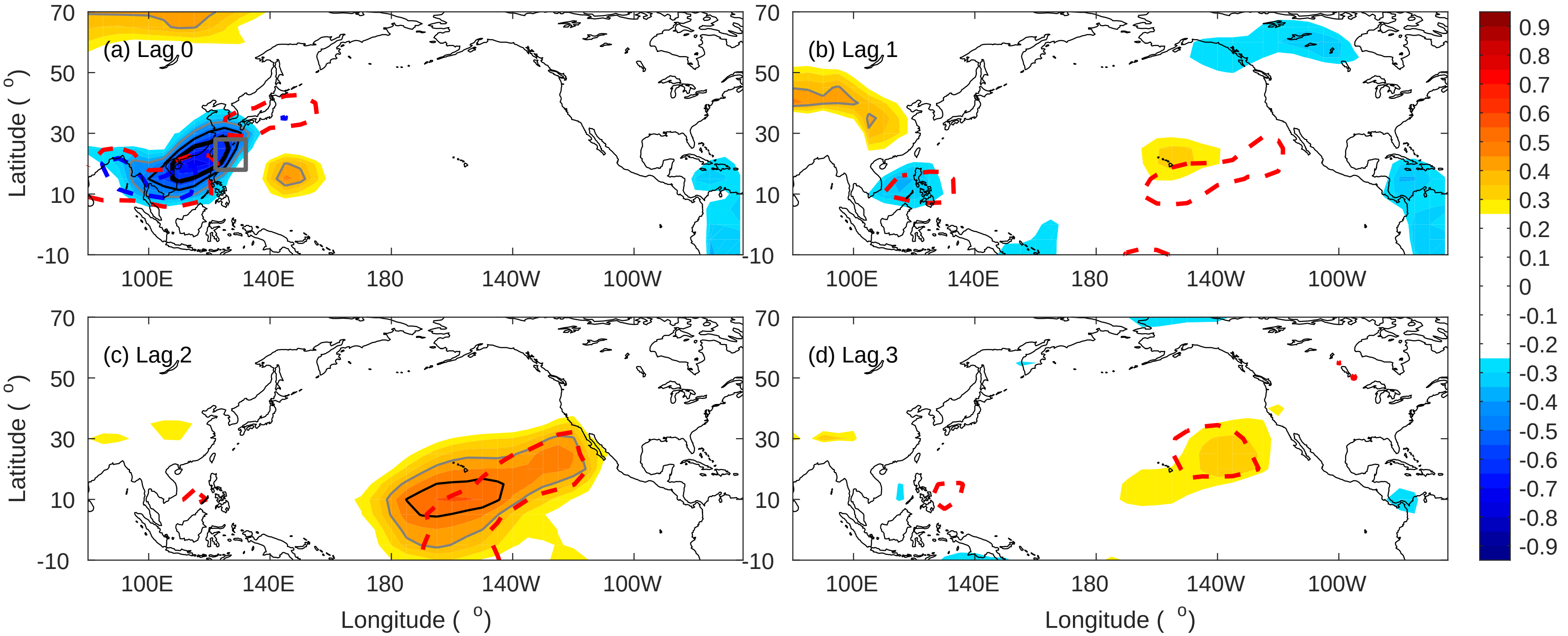

Figure 3. Correlation map of the November surface meridional wind anomaly (V_{PAMS}) in the PAMS with several lags of SLP anomalies (0 to 3 months); (a) November (no lag), (b) December, (c) January and (d) February. See Figure 1 for the description of contour lines. The SST index defined in Wang et al. (2012) is shown as the grey box in (a). Additional thick dashed contours represent similar lag correlations of SLPa with the November SSTa index (Wang et al., 2012) for R= 0.5 (blue) and 0.4 (red).

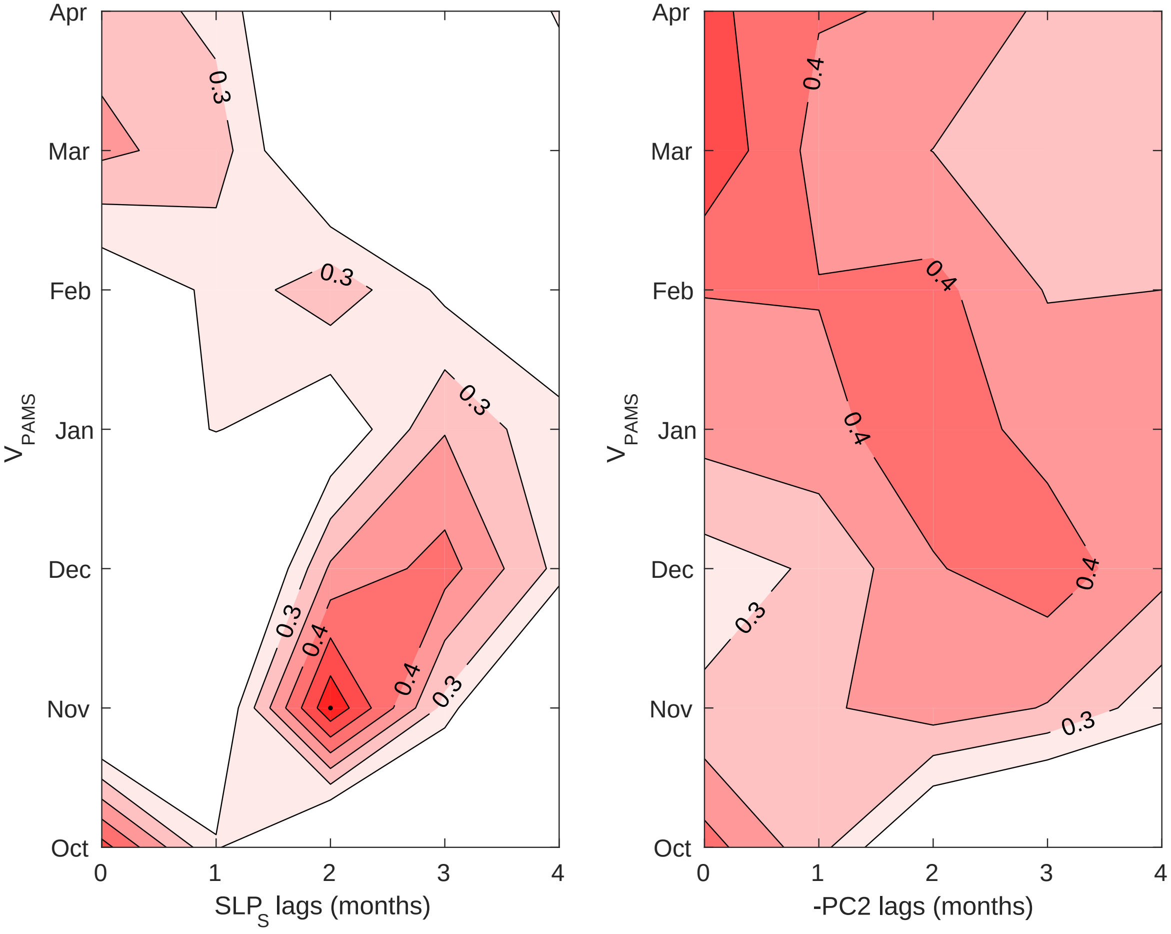

Figure 4. Observed lead–lag correlation between the monthly meridional wind anomalies in PAMS (110~140°E, 5~25°N) and (a) the SLP$_S$ and (b) -PC2, respectively. The SLP$_S$ represents the SLP anomalies in the grey box shown in Figure 1c. See text for the detailed definition of the SLP$_S$ and -PC2. $p<0.05$ is shaded.

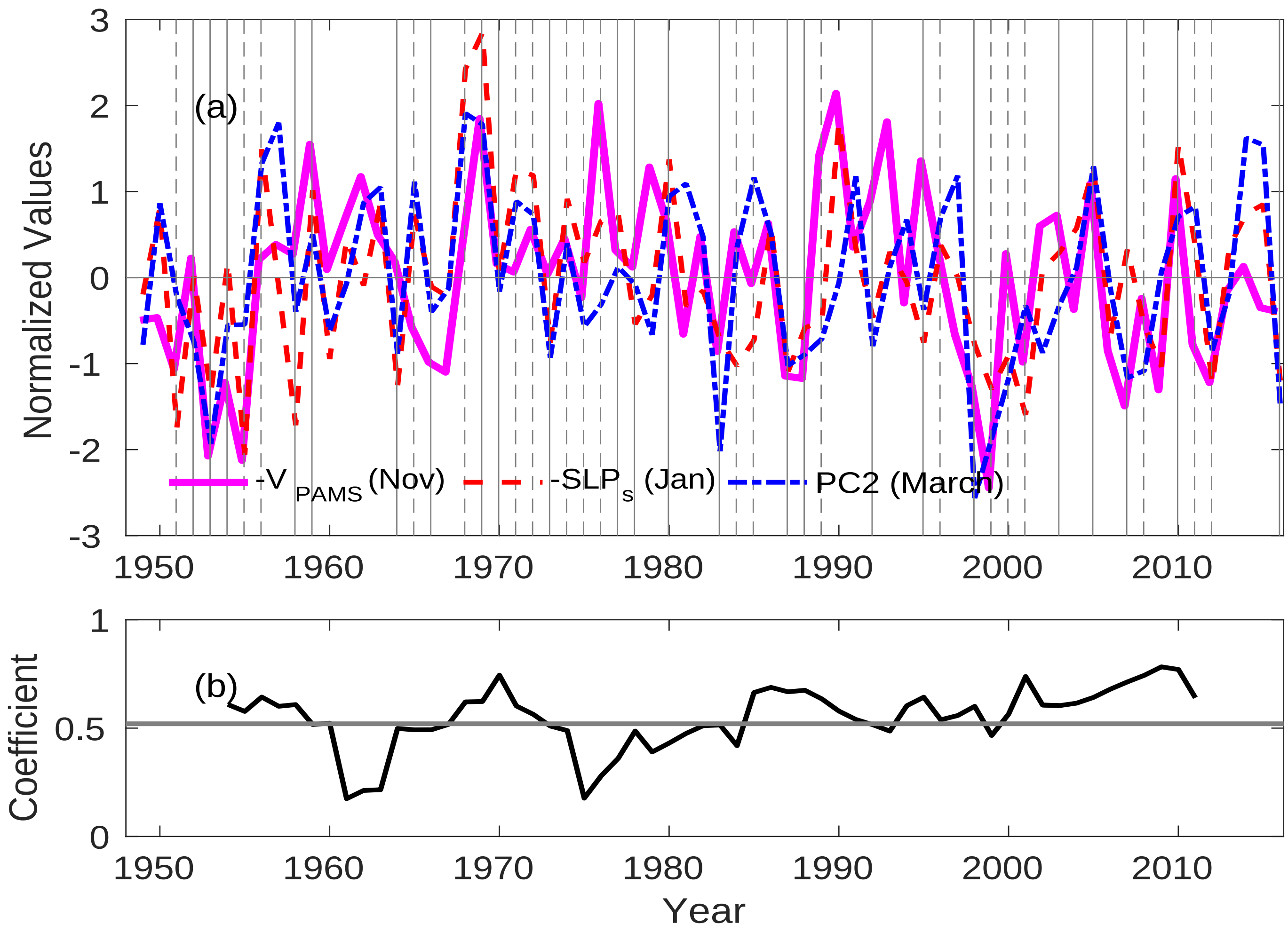

Figure 5. (a) Time series of November equatorward meridional wind anomalies (-V_{PAMS}) in the PAMS (superimposed by January -SLP_S and March PC2, respectively). All time series are aligned with their corresponding months. Black solid (dashed) lines label the El Niño (La Niña) years in December. (b) 11-yr running correlation coefficient between November V_{PAMS} and January SLP_S. The horizontal line indicates the 95% confidence level.

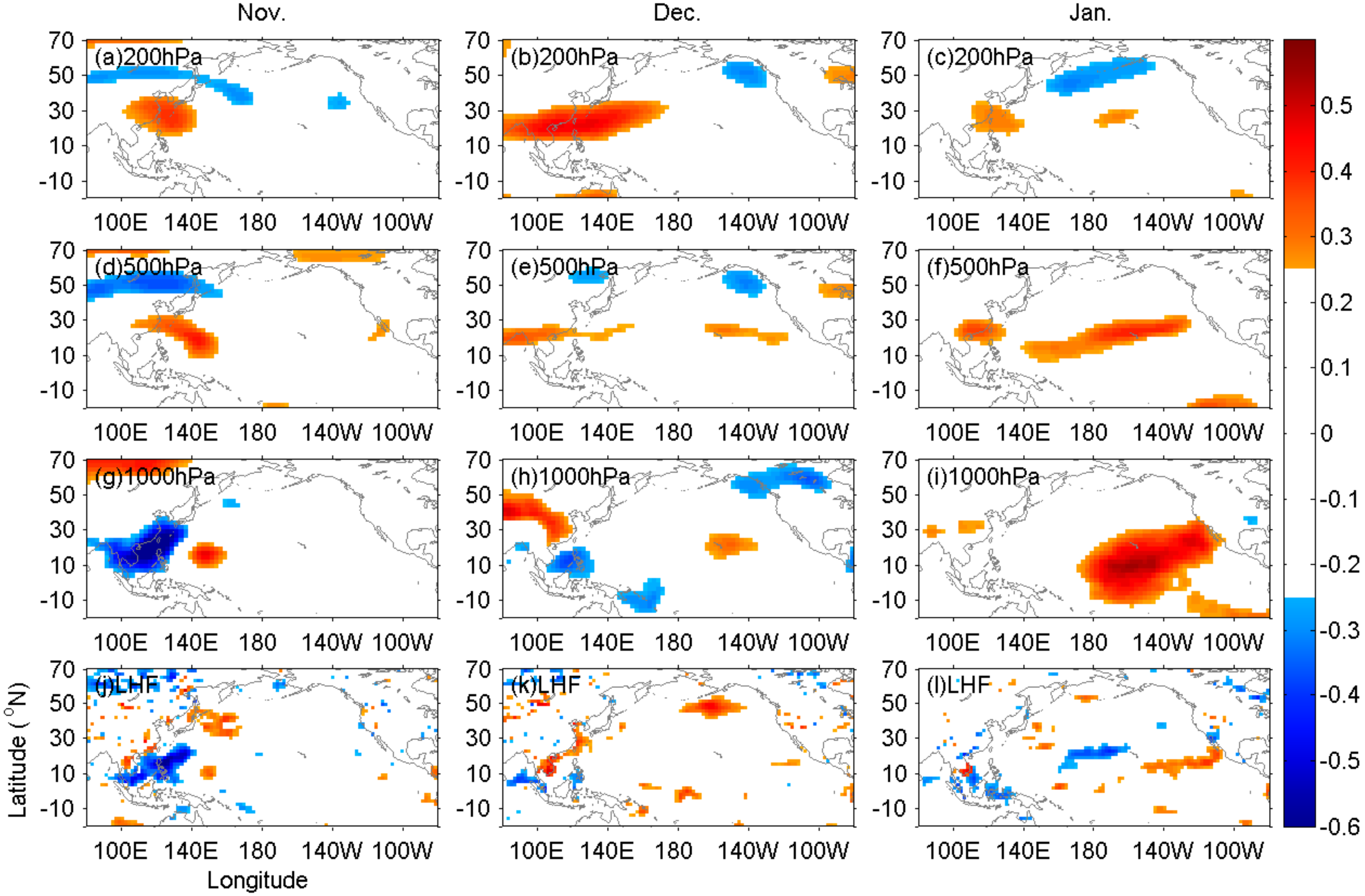

Figure 6. Correlation maps between November meridional wind anomalies (V_{PAMS}) in PAMS and the geopotential height anomalies (top three panels: 200 hPa, 500 hPa and 1000 hPa, respectively) for November and two lag months (December and January). The same correlation maps with latent heat flux at different lag months are shown at the bottom panel. Only $p<0.05$ is shown.

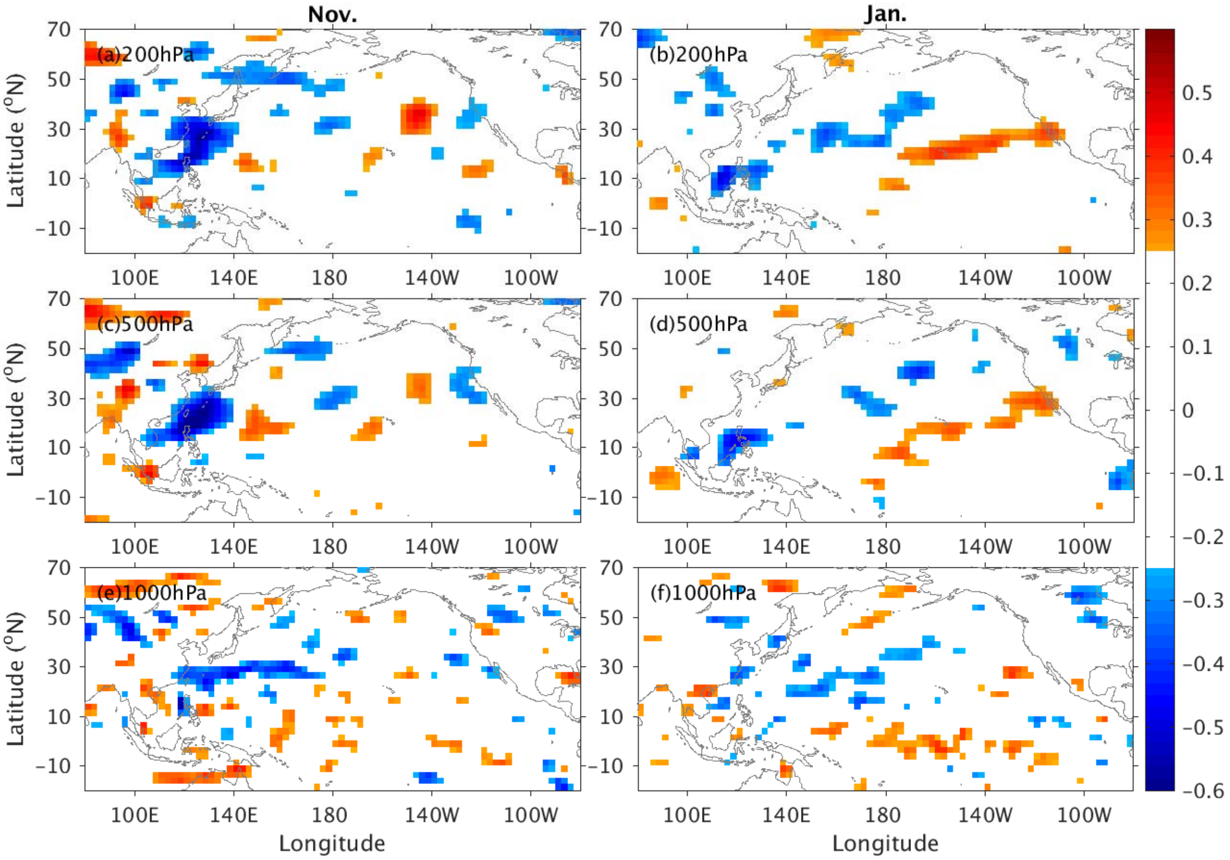

Figure 7. Same as Figure 6 but for the vertical velocity (Ω) anomalies in November (no lag) and January (two month lag).

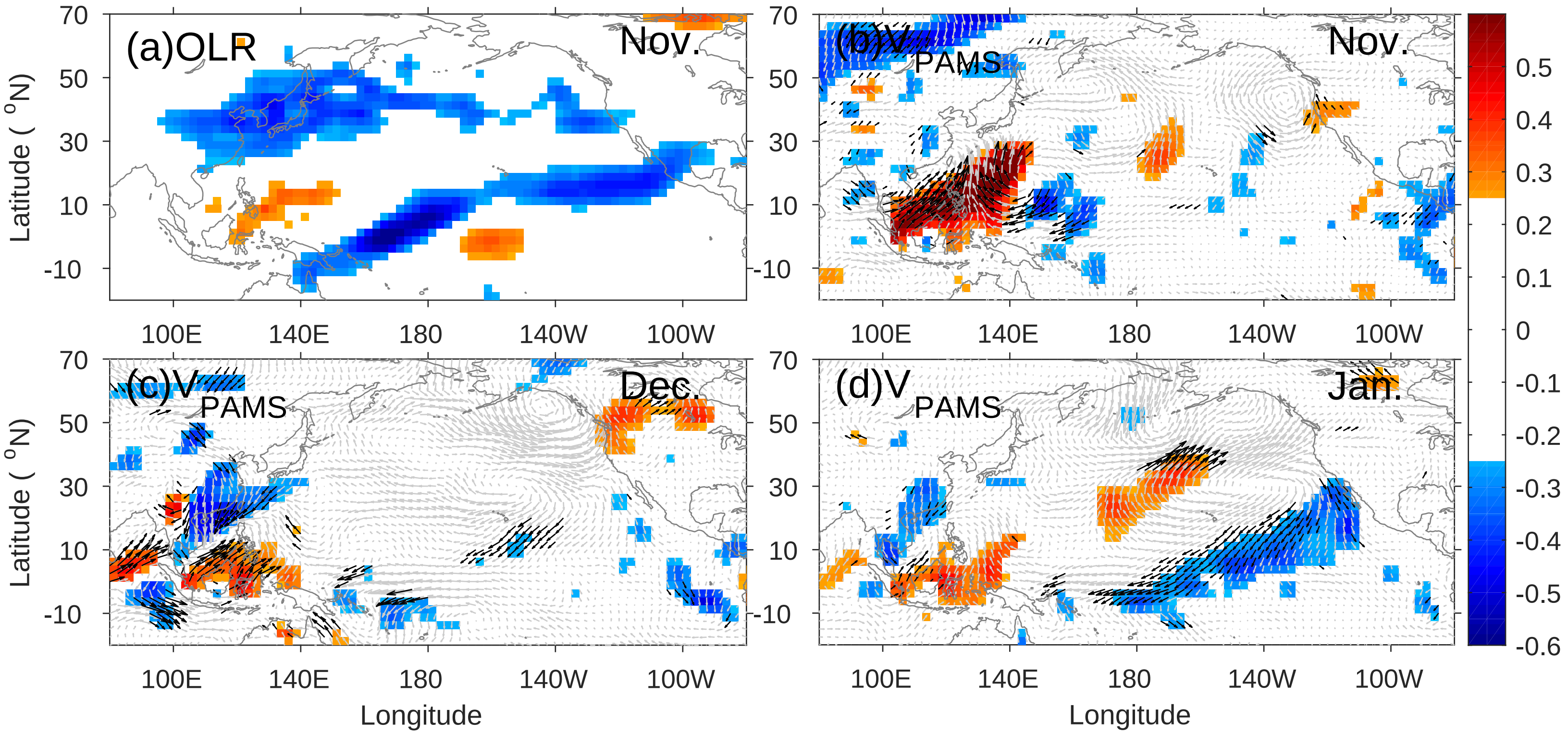

Figure 8: Same as Fig. 6 but for the November OLR anomalies and meridional wind anomalies. Regressions of surface winds onto the V_{PAMS} are superimposed. $p<0.05$ is shown as black.

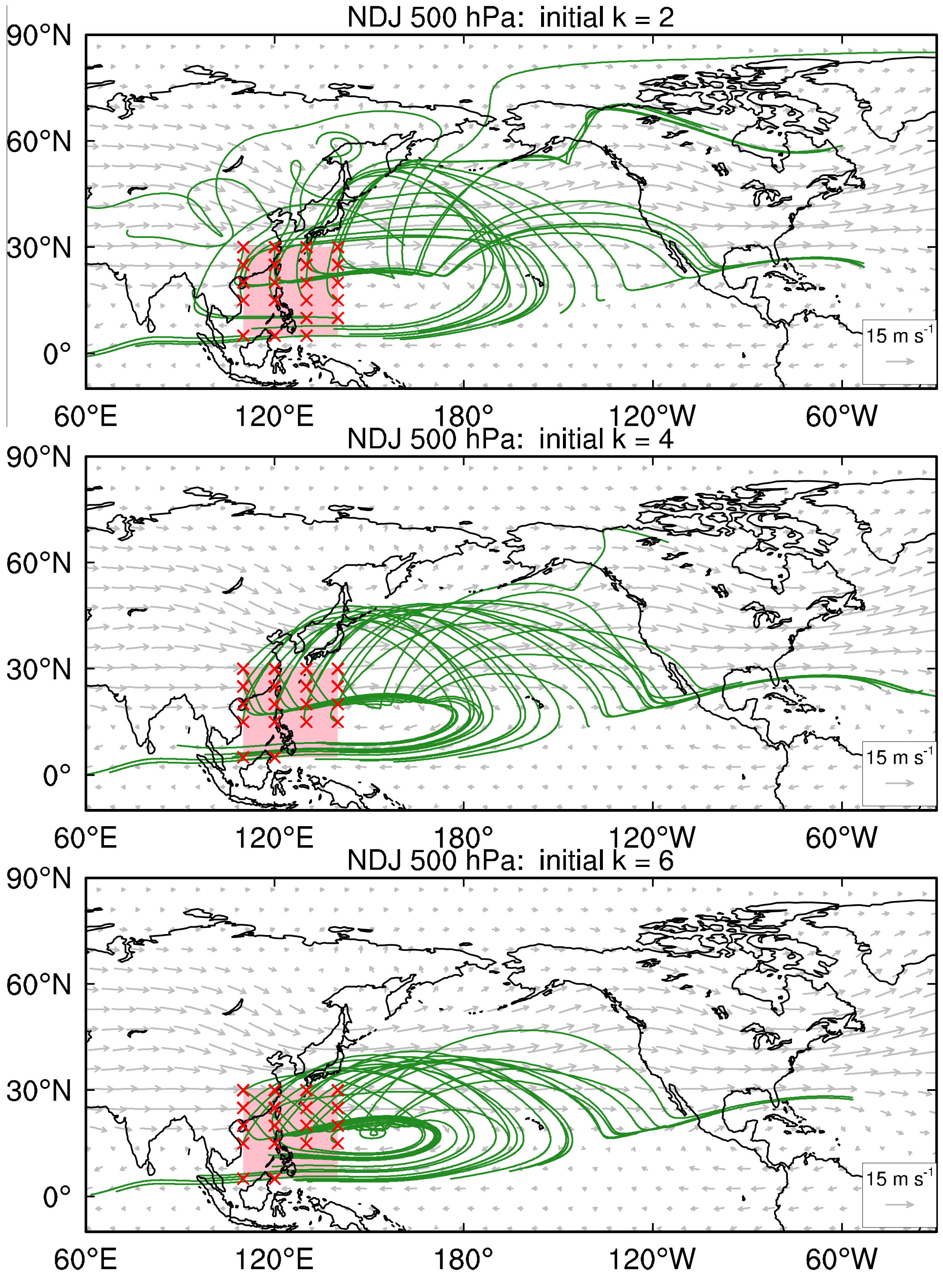

Fig. 9. The stationary Rossby wave ray trajectories (green curves) with initialed zonal wavenumber k = 2, 4, 6 (upper, middle, bottom) under the NDJ (right panels) 500 hPa climatological flows (gray vectors) for the period of 1965-2012. Red forks over pink shadings denote wave source arrays over the PAMS region (110°E-140°E, 5°N-30°N).

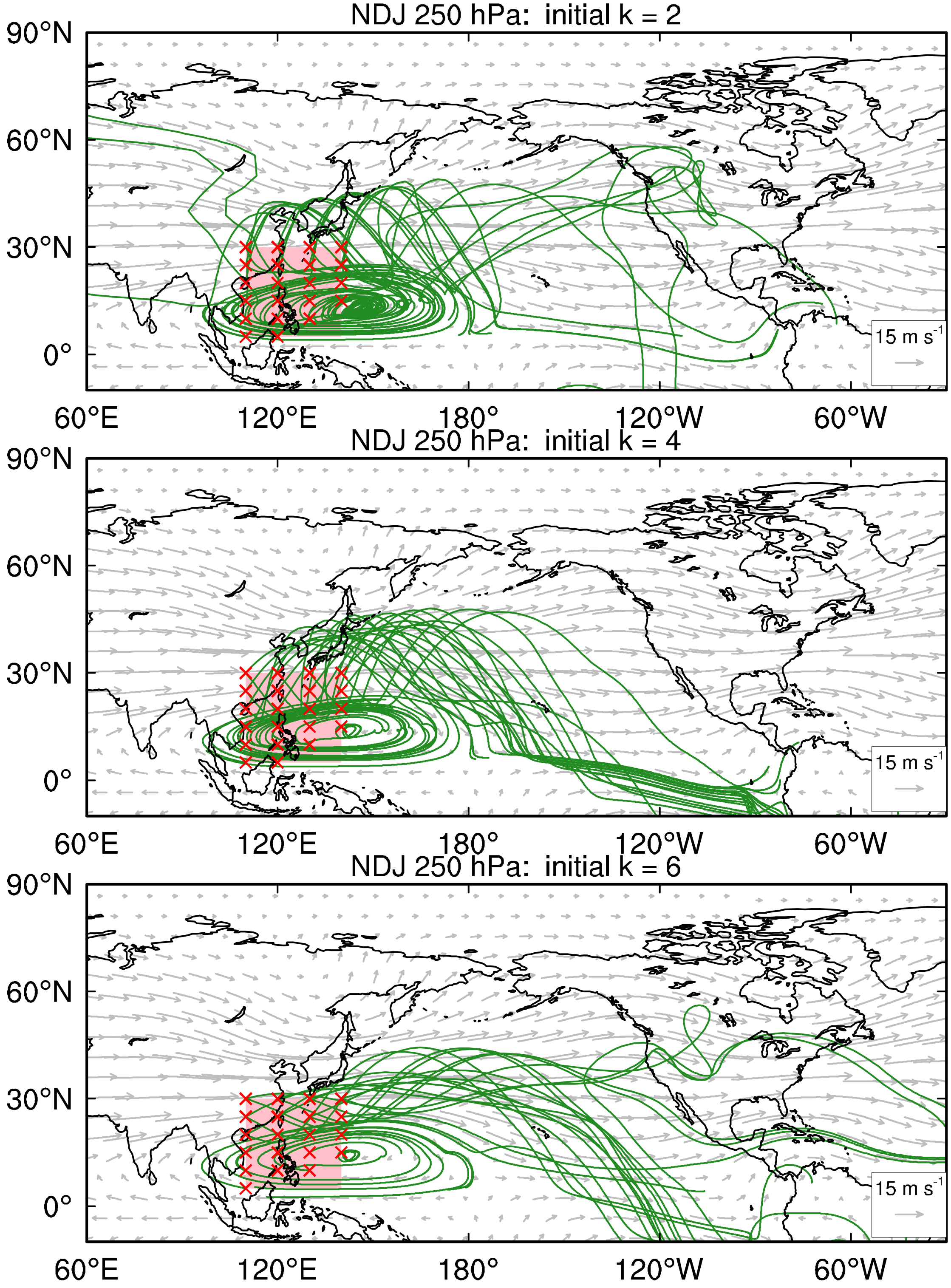

Fig. 10. Same as Fig.9, but for the 250 hPa climatological flows.

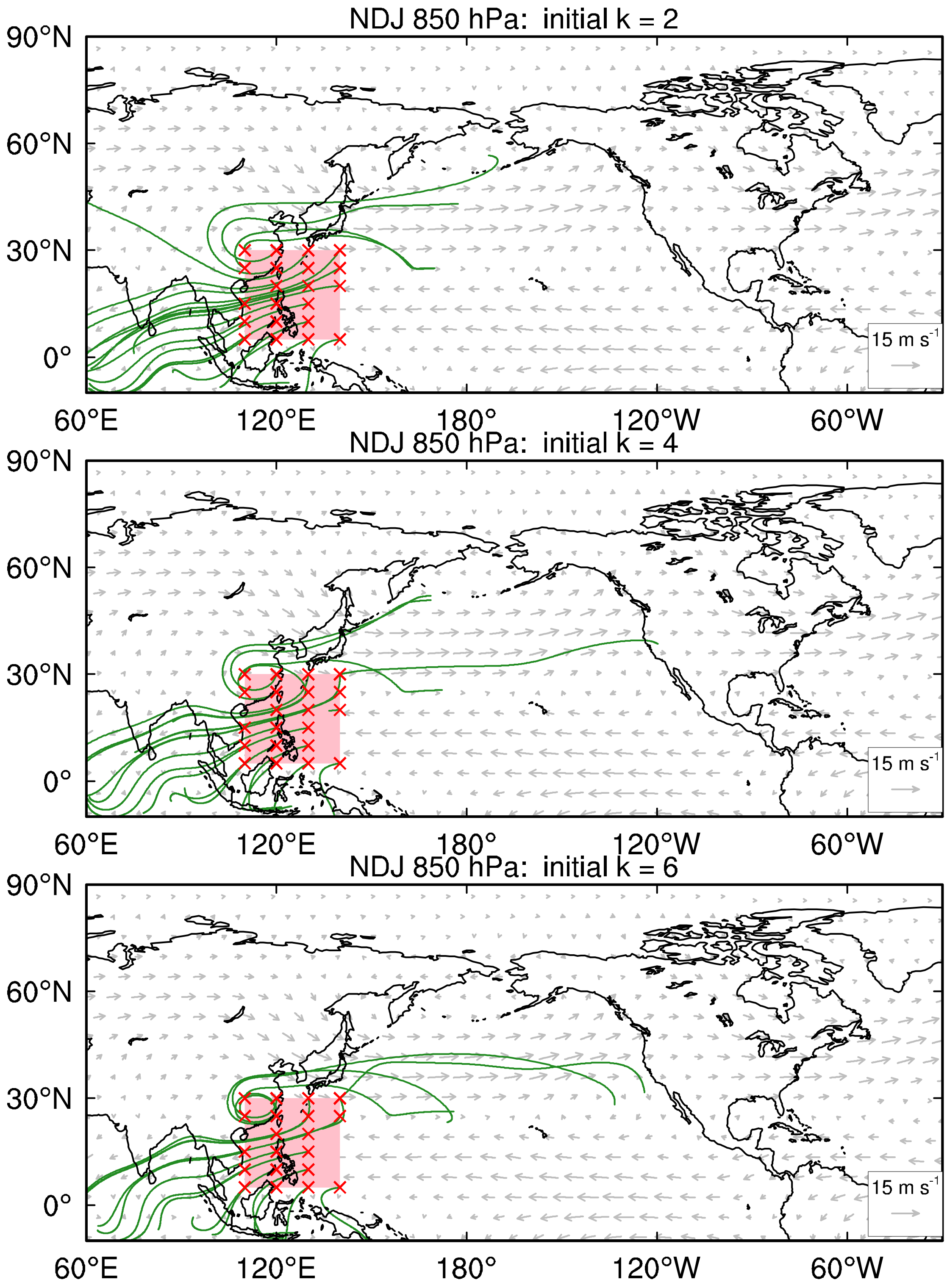

NDJ 850 hPa: initial k = 2

NDJ 850 hPa: initial k = 4

NDJ 850 hPa: initial k = 6

Fig. 11. Same as Fig.9, but for the 850 hPa climatological flows.

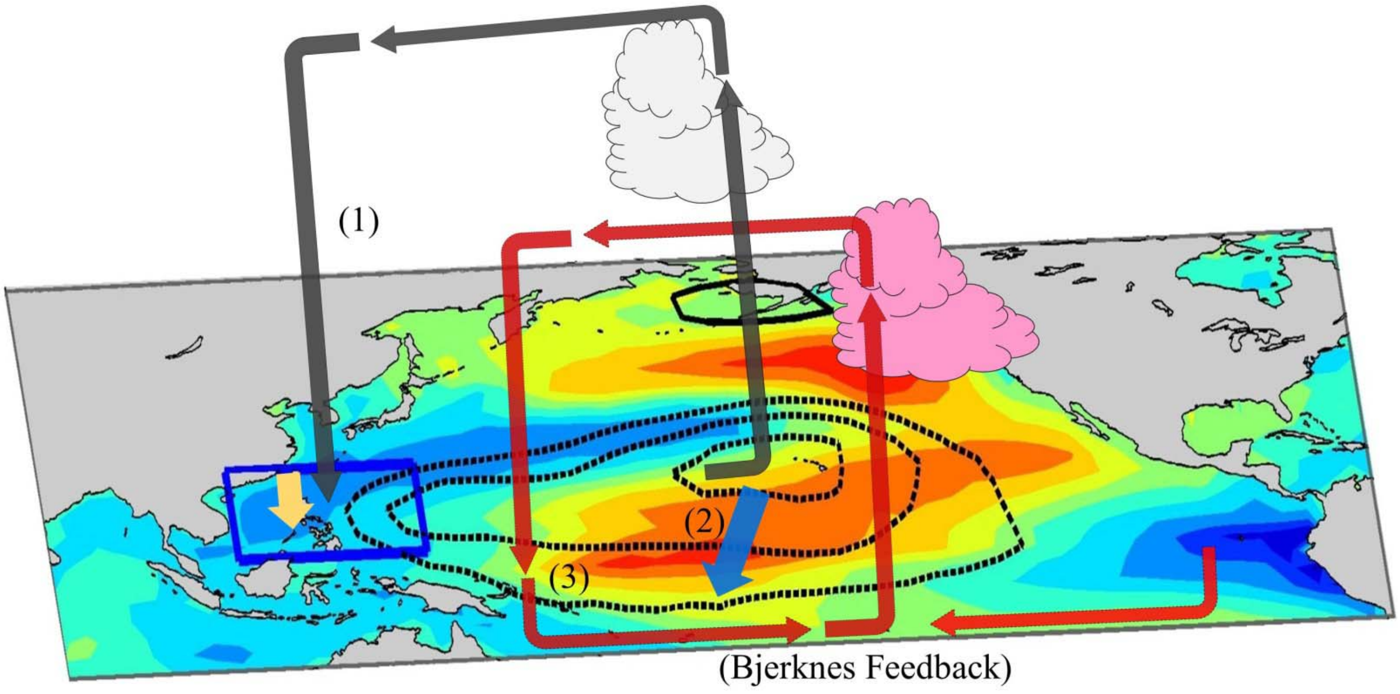

(1) Win(0)-spr(0): equatorward winds in PAMS region (heat flux) → reduced deep convection in PAMS → northeastward propagation → enhanced deep convection near the south branch of the VM (south lobe of the NPO) → enhanced negative phase of NPO

(2) Spr(0)-Sum(0): negative phase of NPO forced VM/MM (CEOF2)

(3) Sum(0)-win(1): enhanced westerly wind in the tropical-subtropical WNP → El Niño

Figure 12. Schematic diagram of the dynamical processes linking the PAMS origin and the onset of El Niño. The SLP (contours) and SST (color) anomalies associated with CEOF2 patterns are overlaid.